Journal of Inorganic and Organometallic Polymers and Materials (2021) 31:3368–3377
https://doi.org/10.1007/s10904-021-01954-x

Effects of Various Transition Metals on the Thermal Oxidative Stabilization of Polyacrylonitrile Nanofibers

Jung-Hun Lee[1] · Siying Li[1] · Ji-Beom Yoo[1,2] · Young-Jun Kim[1,3]

Received: 29 December 2020 / Accepted: 15 February 2021 / Published online: 15 March 2021

Abstract

In this paper, the polyacrylonitrile (PAN) nanofibers and PAN nanofibers bonded with different transition metal (Fe, Co, Ni, and Cu) acetates were successfully prepared and their thermal oxidative stabilization process were analysed by Fourier-transform infrared spectra (FT-IR) and differential scanning calorimetry (DSC). The structural evolution of process was characterized by examining the FTIR spectral peaks generated at four different thermal oxidative stabilization temperatures. Based on the thermal oxidative stabilization rates obtained from each transition metal, Co-PAN and Cu-PAN are the only effective precursors for the thermal oxidative stabilization process and, according to differential scanning calorimetry, Co-PAN is the most effective and suitable precursor for the PAN with different transition metals. Although Co-PAN increased the exothermic reaction (ΔH) by approximately 140%, it alleviates the heat release rate (ΔH/ΔT) by approximately 44%.

Graphic Abstract

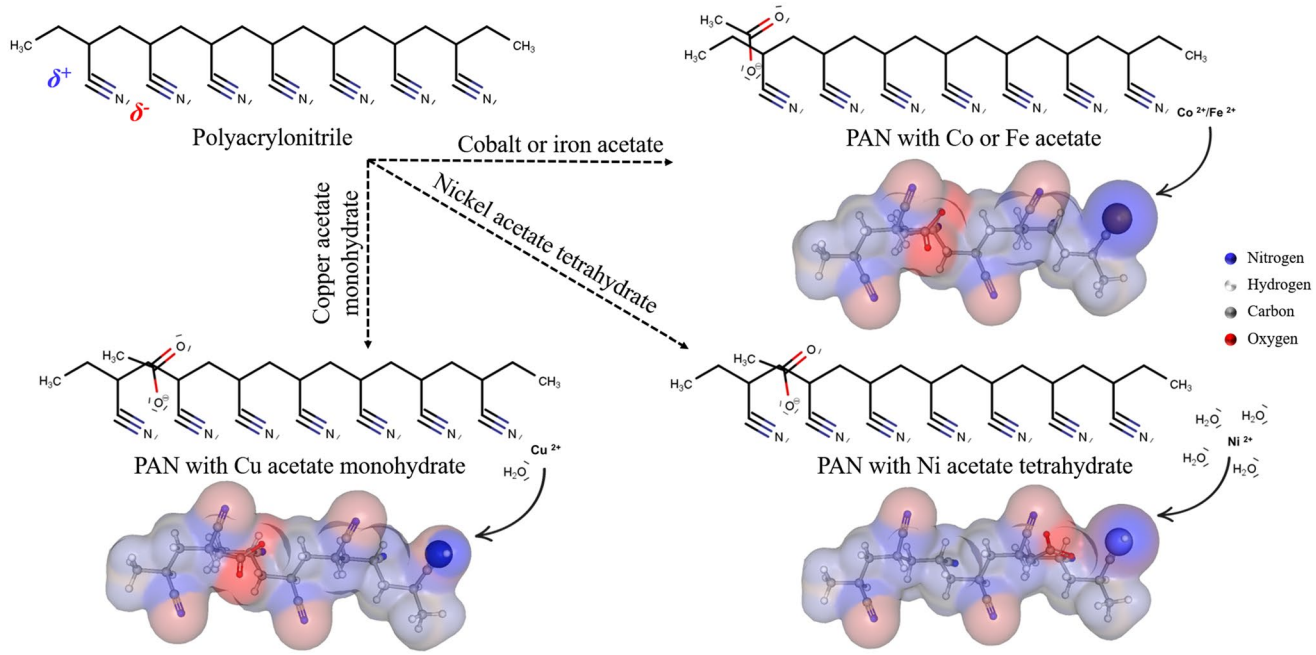

Keywords PAN nanofibers · Transition metal · Thermal oxidative stabilization · Cyclization

Jung-Hun Lee and Siying Li contributed equally to this work.

Extended author information available on the last page of the article

1 Introduction

Polyacrylonitrile (PAN) is one of the most commonly used materials for the fabrication of carbon fibers [1–3]. To produce PAN-based carbon fibers, the polymer must first be converted to a flame-resistant structure (e.g., a ladder-like structure or a non-plastic cyclic structure) through a stabilization process [2] to prevent it from melting during carbonization. The stabilized PAN structure, which has a high rate of conversion to carbon fiber, is the reason why the PAN-based carbon fiber has outstanding properties compared with carbon fibers based on any other precursor material [4, 5].

When heated from 200 to 300 °C in air, PAN will be transformed into a ladder-like structure through cyclization, dehydrogenation, and oxidation processes [4–6]. The cyclization process converts the nitrile groups to conjugated nitrogen double bonds, which in turn forms an aromatic ring together with five carbon atoms [7]. The dehydrogenation process exhausts the hydrogen atoms by reacting with O_2 to form H_2O. Finally, the oxidation of PAN generates oxygen-containing groups, such as carbonyl and carboxyl groups. These reactions lead to the ladder-like structure of PAN and prevent it from melting during carbonization [8].

The structural conversion of PAN releases a large amount of heat, as the formation of free radicals that initiate cyclization leads to a sudden and rapid evolution of thermal energy [7, 9, 10]. Since the intense exothermic reaction can break the molecular chain of PAN, the resultant carbon fibers are left with inferior characteristics. To alleviate the intense exothermic reaction, researchers have tried to blend PAN with different co-monomers and reported the effects on the cyclization kinetics. For example, to decrease the stabilization temperature and/or alleviate the intense exothermic reaction, PAN was copolymerized with itaconic acid (IA), acrylic acid (AA), ammonium salt of itaconic acid (AIA), guanidinium itaconate (GIA), methyl acrylate (MA), methacrylic acid (MAA), or 2-acrylamido-2-methylpropane acid (AMPS) [9–18]. Among these co-monomers, IA resulted in a significant decrease in the stabilization temperature and alleviated the intense exothermic reaction [14, 16–18]. Unfortunately, it also decreased the cyclization rate, generating many beta-amino groups and conjugated nitrile groups, which caused point defects in the carbon fiber [19, 20]. Moskowitz et al. reported GIA contained copolymers showed a significant reduction in heat flow and cyclization peak temperature as compare to IA copolymers.

In addition to organic materials, inorganic materials such as carbon nanotubes (CNTs) and functionalized CNTs have been mixed with the PAN precursor [7, 21, 22]. CNTs enhance the mechanical properties of the carbon fiber. Since PAN is already a one-dimensional crystallized material consisting of carbon atoms, it can easily stack upon the CNTs to form a graphitic structure. In other words, the CNTs in the PAN work as nucleation sites for graphitic structure formation [22]. However, the CNTs had a negative effect on the PAN stabilization process as the stabilization of the PAN–CNTs composite resulted in more unreacted nitrile groups than the stabilization of PAN alone. Therefore, the composite required a relatively longer stabilization time [22].

Over the years, the synthesis and application of metal and metal oxide nanoparticles have attracted the interest of a wide range of researchers from different fields [23–28]. As another kind of inorganic additives, the study of applying transition metals and their oxides in PAN fibers by adding transition metal salts in PAN solutions for electrospinning has received much attention [28–33]. Co nanoparticles encapsulated in PAN-based carbon fibers were applied as electrocatalysts for the stable oxygen reduction reaction [28]. A core–shell structure assembled by $Ni(OH)_2$ grown on $NiCo_2O_4$ embedded PAN-based carbon nanofibers (CNFs) was successfully synthesized and applied as anode material in a supercapacitor [29]. Functionalized porous graphitic CNFs incorporated with iron acetylacetonate sacrificial catalyst performed exceptional rate performance in lithium-ion batteries as anode material [30]. Activated CNFs composite with Cu/Cu_xO nanoparticles prepared by electrospinning of copper acetate addicted PAN solution followed by carbonization and mild activation was fabricated and its enhanced adsorption to gaseous pollutant H_2S was investigated [31]. Although there are diverse studies on the applications of transition metal and metal oxide nanoparticles composite with PAN CNFs, there is a lack of studies on the reaction of metal salt additions with PAN during synthesis and subsequent stabilization.

Usually, transition metals can be used to reduce the activation energy of a reaction, resulting in a higher reaction rate. Therefore, in this study, we investigated the effects of several transition metals on the PAN stabilization process using differential scanning calorimetry (DSC) and Fourier-transform infrared (FTIR) spectroscopy. For this purpose, we used the acetate salts of iron (Fe), cobalt (Co), nickel (Ni), and copper (Cu). Each transition metal resulted in a different cyclization rate, exothermic reaction, and enthalpy during the PAN stabilization process.

2 Experimental

2.1 Materials

PAN (average Mw 150,000) and *N*,*N*-dimethylformamide (DMF) were purchased from Sigma-Aldrich Korea Co., Ltd. (Republic of Korea). Likewise, copper acetate monohydrate (CAS No. 6046-93-1), iron acetate (CAS No. 3094-87-9),

nickel acetate tetrahydrate (CAS No. 6018-89-9), and cobalt acetate (CAS No. 71-48-7) were purchased from Sigma-Aldrich Korea Co., Ltd. These transition metal salts and PAN were first dissolved in DMF separately as shown in Fig. S1 (a) in the supplementary information, and then they were dispersed into each other to form a 10 wt% of PAN and 0.1 wt% of transition metal salts in DMF (PAN: metal ion = 99:1) as shown in Fig. S1 (b) in the supplementary information.

2.2 Electrospinning

The electrospinning setup consisted of a positively charged needle nozzle with a high-voltage DC power supply (Nano NC Co. Ltd., Republic of Korea). The feed rate and applied voltage were 0.05 mL h^{-1} and 10 kV, respectively. The electrospun fibers were deposited onto a rotating aluminum drum collector at 485 rpm.

2.3 Thermal Oxidative Stabilization

PAN stabilization was carried out with the thermal oxidative stabilization. The furnace was set at four different temperatures: 200 °C, 240 °C, 280 °C, and 320 °C. The fibers were heat treated for 1 h in air with a temperature increasing rate of 2 °C min^{-1}.

2.4 Characterization

A scanning electron microscope (SEM; JSM-7401F, JEOL, Japan) was used to observe the withdrawn fibers. FTIR spectrometer (Nicolet iS5, Thermo Fisher Scientific, Waltham, MA, USA) was used to analyze changes in the chemical composition of the stabilized PAN. Each sample was scanned 32 times at a resolution of 4 cm^{-1}. DSC analysis was performed to measure the heat released during the stabilization process. The conformation of PAN molecules bonded with the transition metal precursors were visualized using Marvin Sketch (ChemAxon Ltd., Budapest, Hungary).

3 Results and Discussion

The conformation of PAN molecules bonded with various transition metal precursors were visualized to identify how the transition metal ions affect the stabilization of the polymer (Fig. 1a). Owing to the polarity of the

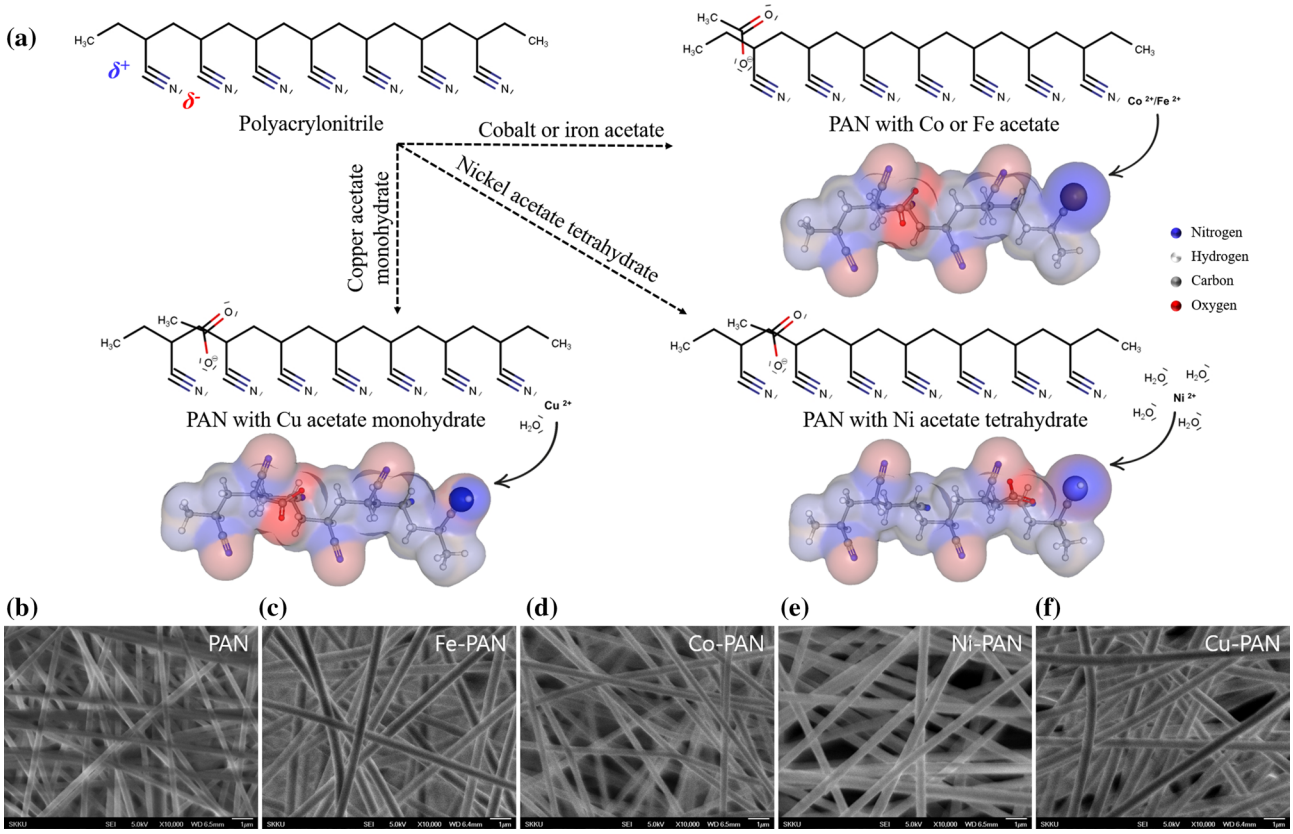

Fig. 1 **a** Two-dimensional and three-dimensional conformer structures of polyacrylonitrile (PAN) with cobalt acetate, iron acetate, copper acetate monohydrate, and nickel acetate tetrahydrate. SEM images of as-spun PAN nanofibers **b** without transition metal acetate, **c** with ion acetate, **d** with cobalt acetate, **e** with nickel acetate tetrahydrate, and **f** with copper acetate monohydrate

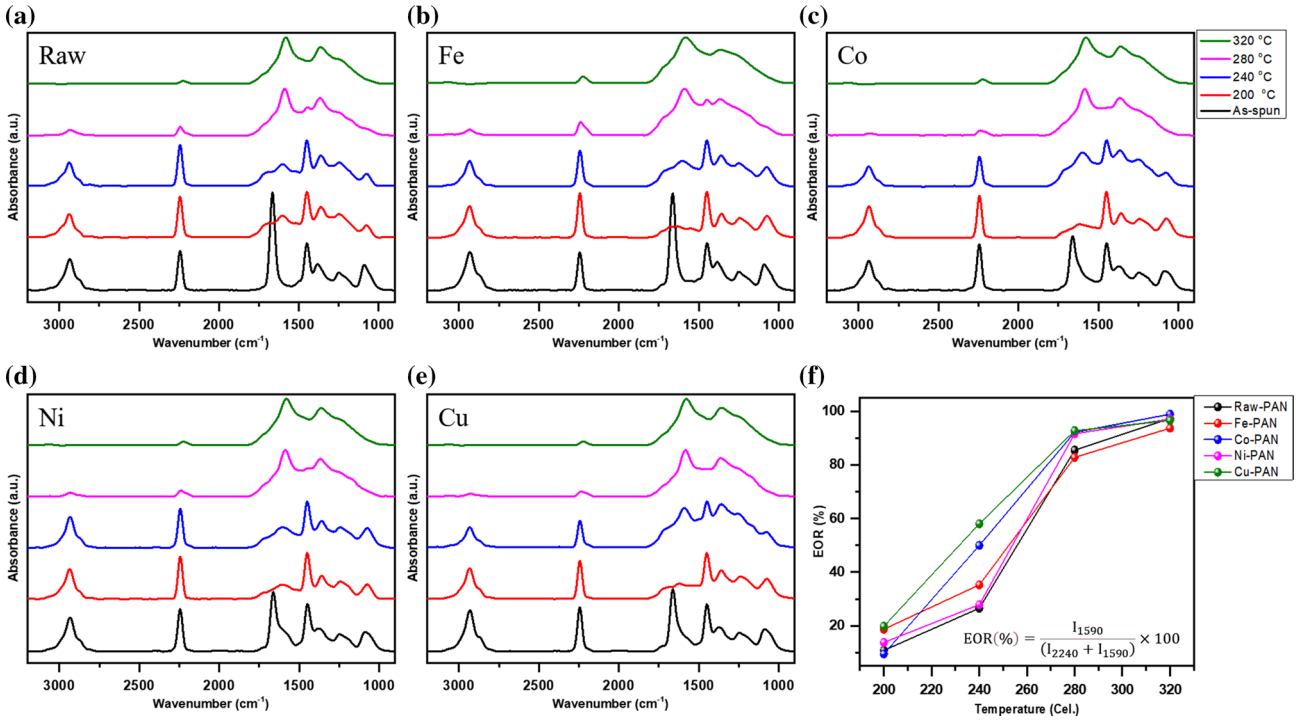

Fig. 2 FTIR peaks of PAN bonded with transition metal ions according to the various stabilization temperatures. **a** Raw PAN; **b** PAN with iron acetate; **c** PAN with cobalt acetate; **d** PAN with nickel acetate tetrahydrate; **e** PAN with copper acetate monohydrate; **f** extent of the cyclization reaction ratio (EOR) of PAN with different metal ions according to the stabilization temperature

acetate from the transition metal precursors, the opposite charge of the carbon side of the nitrile groups attracts the carboxyl groups of acetate. As shown in Fig. 1a, since the nitrile groups in PAN have high polarity, the Co^{2+}, Fe^{2+}, and Cu^{2+} ions are attracted to the negatively charged nitrogen side. However, because the Ni^{2+} ions are surrounded by negatively charged water molecules, they are prevented from bonding with the nitrile groups of PAN. Therefore, the positively charged metal ions would affect the redox properties of the polymer. The microstructure of as-spun PAN and PAN bonded with various transition metal ions were confirmed by SEM and showed in Fig. 1b–f.

The FTIR spectra of the as-spun PAN and PAN bonded with the various transition metal ions fibers at different stabilization temperatures are presented in Fig. 2. The identities of the peaks are summarized in Table 1. The FTIR spectrum of the as-spun PAN exhibited characteristic peaks in the range of 2850–2940 cm^{-1} for the asymmetric vibration of CH_2 groups ($\nu_{as(CH2)}$), at 2240 cm^{-1} for the vibration peak of the nitrile groups, and at about1650–1680 cm^{-1} for the vibrational mode of the carbonyl groups (C=O highly conjugated from remaining DMF). The addition of the transition metal precursors to PAN slightly increased the broad peak from the carboxyl group ($–COO^-$) in acetate in the range of 1560–1590 cm^{-1}.

During the thermal oxidative stabilization of PAN, the CH_2 backbone (at 2940 cm^{-1}) lost hydrogen atoms and the nitrile (–C≡N) peak turned into peaks for the cyclic –C=N– and –C–N– groups. With an increase of the stabilization temperature, the nitrile peak at 2240 cm^{-1} disappeared and a broad peak of the –C=N–, –N–H–, and C=C groups appeared at about 1590 cm^{-1}. At the same time, the intensity of the O–H and N–H stretching peaks (at 3370 and 3324 cm^{-1}, respectively) gradually appeared with increasing temperatures. The tautomerization of PAN is generated and initiated by oxygen (in the air) [10, 11], which accepts the lone pair of electrons from the nitrile groups and dehydrogenates the polymer. The dehydrogenation process generates free radicals in the PAN molecules, which bind with oxygen to become the carbonyl groups ($\nu_{C=O}$ peaks at 1700 and 1650 cm^{-1}). In this way, PAN turns into a ladder-like structure that makes it non-flammable. Since this reaction occurs at 200–300 °C, we annealed the PAN molecules with transition metals at the temperatures of 200 °C, 240 °C, 280 °C, and 320 °C in air.

Even though the nitrile groups turned into the cyclic structure in all samples, the reaction rates were different depending on the assisting transition metal precursor and the stabilization temperature. The extent of ratio (EOR) for the cyclization reaction was calculated as follows [46]:

Table 1 Interpretation of the FTIR absorbance peaks of PAN and PAN bonded with different transition metal ions during the thermal oxidative stabilization process

As spun PAN					After stabilization				
Wavenumber (cm^{-1})	Group	Vibration type	Assignment	Refs.	Wavenumber (cm^{-1})	Group	Vibration type	Assignment	Refs.
1070–1080	C–CN	ν_{C-CN}		[10, 14]	1070–1080	C–CN	ν_{C-CN}		[10, 14]
1080–1100	CH		Aliphatic ethers, alcohols	[34]	1160–1190	C–O–	ν_{CO}	α, β-unsaturated esters and carboxylic acids	[10, 14]
1190–1200	C=O		C–O group in α, β-unsaturated esters and carboxylic acids	[14]	1230–1260	C–O, C–C, C–N, C–O–C	ν_{C-O}, ν_{C-C}, ν_{C-N} $\nu_{asC-O-C}$ in ether		[10, 14]
1245–1255	C–O	ν_{CO}		[14]	1290–1330	C–O–, COO	δ_{C-O}, $\delta_{CH2,}$ ν_{asCOO}		[14, 35, 36]
1310–1320	C–O–	δ_{C-O}, $\delta_{CH2\ at\ C-6}$		[14, 35]	1360–1370	C–H + N–H + OH	$\delta_{C-H} + \delta_{N-H} + \delta_{O-H}$	C–H, N–H, O–H in ring	[14, 35]
1340–1365	CH	δ_{C-H}		[14]	1420–1450	C–H	δ_{sC-H}	In CH_2	[10, 14, 34, 36, 37]
1375–1395	C–H, N–H, O–H	$\delta_{C-H} + \delta_{N-H} + \delta_{OH}$		[10, 21, 38]	1490–1510	C=C	$\upsilon_{C=C}$	Of ring, Tyr–O^- or Trp	[10, 39, 40]
1450	CH_2	δ_{CH} flat	CH_2 bending (scissoring)	[10, 14, 37]	1520–1540	C–N, CH, N–H	$[\nu_{s(CN)} + \delta_{(CH)}]_{ring} + \delta s_{(NH3)}$	Tyr–OH, amide	[10, 41, 42]
1560–1590	$–COO^-$		Carboxyl group in salt from $–COO^-$	[34]	1590–1620	C=C, C=N, N–H	$\nu_{C=C} + \nu_{C=N} + \delta_{N-H}$	Cyclic structure originated from cyclization and dehydrogenation reactions	[10, 43]
1620	RCOO–	ν_{asC-O}	Carboxylate anion	[14]	1640–1660	C=O		Highly conjugated, acridone ring	[34, 41]
1650–1680	C=O, C=C, C=N	$\nu_{C=O,}$ $\nu_{C=C} + \nu_{C=N}$	C=O highly conjugated (from DMF)	[34] [10]	1700–1730	C=O	$\nu_{s(C=O)}$	Ketone, aldehyde, and –COOH	[10, 34, 39]
1710	RCOOR′	Stretching	Carbonyl group in α,β-unsaturated esters	[14]	2170–2190			β-amino	[14, 20, 21, 44]
1730	RCOOH	Stretching	Carbonyl group in α,β-unsaturated acids	[14]	2200–2220			Conjugated nitrile	[14, 20, 21, 44]
2240–2243	C≡N		Unreacted nitrile	[14, 21, 38, 44, 45]	2240–2243	C≡N		Unreacted nitrile	[14, 21, 38, 44, 45]
2850–2870	$–O–CH_3$			[14, 35]					
2930–2940	–C–H	Asymmetric ν_{CH2}		[14, 35]					

ν: Stretching vibration; δ: Bending vibration; as: asymmetric; s: symmetric; DMF: *N*,*N*-dimethylformamide

Table 2 Standard hydrogen electrode (SHE)

Oxidant		Reductant	E^0 (V)
$Fe^{2+} + 2e^-$	↔	Fe(s)	− 0.44
$Co^{2+} + 2e^-$	↔	Co(s)	− 0.28
$Ni^{2+} + 2e^-$	↔	Ni(s)	− 0.25
$2H^+ + 2e^-$	↔	H_2(g)	0.0000
$Cu^{2+} + 2e^-$	↔	Cu(s)	+0.337
$Cu^+ + e^-$	↔	Cu(s)	+0.520
$O_2(g) + 4H^+ + 4e^-$	↔	$2H_2O$	+1.229

$$\mathrm{EOR}\,(\%) = \frac{I_{1590}}{(I_{2240} + I_{1590})} \times 100$$

where I_{1590} and I_{2240} are the intensities of the peak related to –C=N–, –N–H–, and C=C groups at 1590 cm^{-1} and of the nitrile peaks at 2240 cm^{-1}.

As shown in Fig. 2, copper acetate monohydrate and cobalt acetate were effective precursors for initiating the stabilization of PAN over all temperature ranges. According to the standard hydrogen electrode (SHE), the effectiveness of the ions in initiating the reaction was predicted to be in the order of Cu > Ni > Co > Fe (Table 2). However, according to the EOR calculation, at 240 °C, the nitrile groups of PAN turned into the cyclic structure in the order of Cu > Co > Fe > Ni (Fig. 2f). The stabilization rate of Ni-PAN increased significantly between 240 and 280 °C, which might be due to the evaporation of the water molecules in the tetrahydrate phase at these temperatures. Moreover, iron acetate hindered the transformation of the nitrile groups into the cyclic structure. Fe^{2+} showed a different behavior from other metal ions in the PAN stabilization process near 1300 cm^{-1}, which was related to oxygen bond in the carboxyl group.

To determine the effect of different transition metal ions on the structural evolution and thermal oxidative stabilization of PAN at 280 °C, FTIR spectral curves of raw PAN and PAN bonded with the transition metal ions were fitted in the range of 1000–2000 cm^{-1}. The fitting curves of the $\nu_{C=O}$ peaks (at 1700 and 1650 cm^{-1}), the $\nu_{C=C} + \nu_{C=N}$ peak (at 1600 cm^{-1}), the $\nu_{C-N} + \delta_{N-H}$ peak of amide (at 1525 cm^{-1}), the δ_{sC-H} peak of CH_2 (at 1450 cm^{-1}), and the ν_{C-CN} peak at 1080 cm^{-1} are shown in Fig. 3. Cu^{2+} and Co^{2+} in PAN reduced the CH_2 backbone peak (at 1450 cm^{-1}) and the C–CN peak (at 1080 cm^{-1}) more than the other metal ions, indicating a higher degree of dehydrogenation. In addition, the $\nu_{C=C} + \nu_{C=N}$ peak (at 1590 cm^{-1}) was much higher than the other fitted peaks, suggesting that more cyclization reactions had occurred. However, the stabilization reaction with Fe-PAN showed a low intensity for the $\nu_{C=C} + \nu_{C=N}$ peak and a high intensity for the CH_2 backbone peak. Because of the low cyclization rate, the peak intensity of $\delta_{C-H} + \delta_{N-H} + \delta_{O-H}$ in the ring (at 1370 cm^{-1}) was also relatively low. In addition, the intensity of the $\nu_{C=O}$ peak at 1700 cm^{-1} in Fe-PAN was higher than that of the other peaks in the other samples.

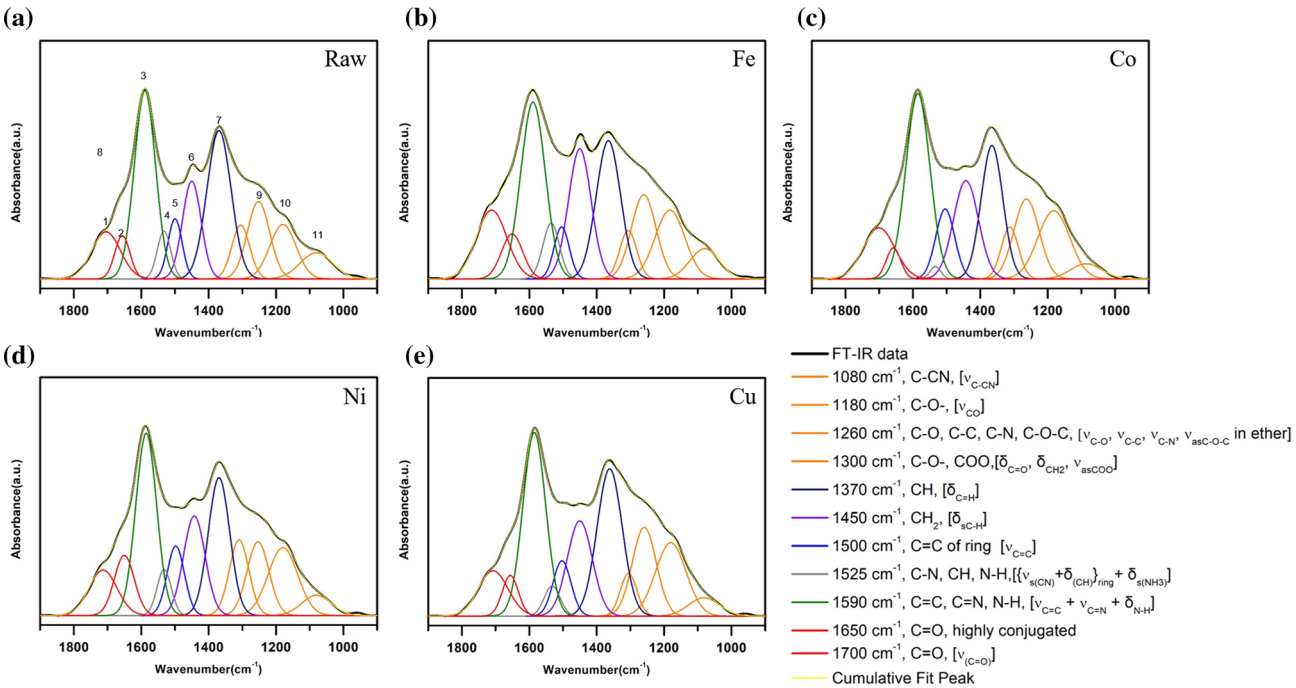

Fig. 3 Peak fitting of FTIR by the Gaussian function in the range of 900–2000 cm^{-1}. **a** Raw PAN and PAN bonded with **b** Fe^{2+}, **c** Co^{2+}, **d** Ni^{2+}, and **e** Cu^{2+}. Thermal oxidative stabilization was carried out at 280 °C

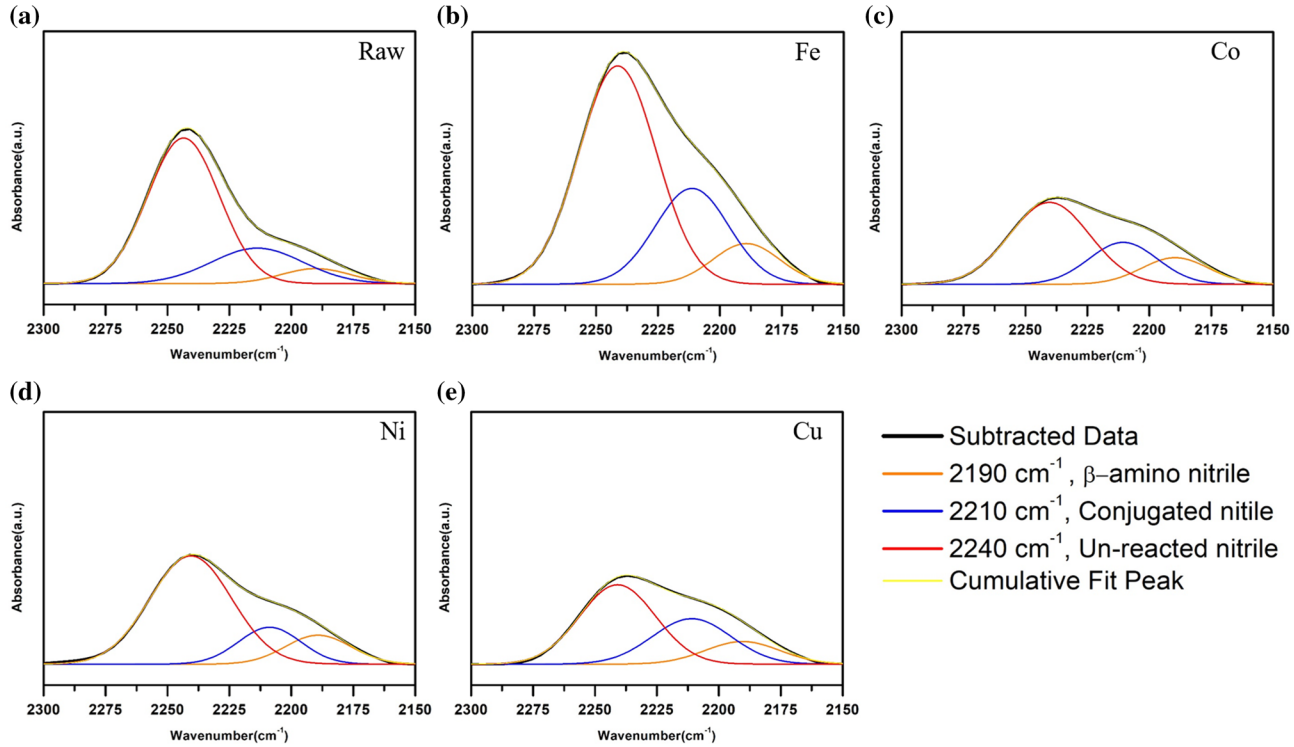

Fig. 4 Peak fitting of FTIR by the Gaussian function in the range of 2150–2300 cm^{-1}. **a** Raw PAN and PAN bonded with **b** Fe^{2+}, **c** Co^{2+}, **d** Ni^{2+}, and **e** Cu^{2+}. Thermal oxidative stabilization was carried out at 280 °C

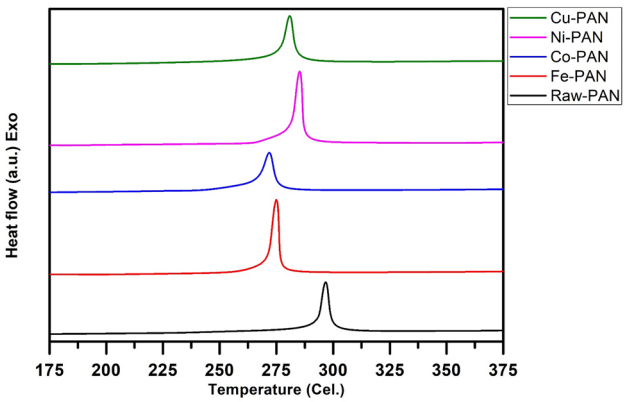

Fig. 5 Differential scanning calorimetry (DSC) thermograms of PAN bonded with various transition metal ions in the air

The C=O peak at 1650 cm^{-1} represents the conjugated carbonyl group in the acridone ring, whereas the C=O peak at 1700 cm^{-1} is for the unconjugated carbonyl group in hydronaphthyridine [10, 14].

The peak fitting of FTIR by the Gaussian function in the range of 2150–2300 cm^{-1} is presented in Fig. 4. Two new peaks at 2190 and 2210 cm^{-1}, identified as β-aminonitrile and conjugated nitrile, respectively, were associated with the transformation of the nitrile peak at 2240 cm^{-1} (Fig. 4). These unsaturated nitrile groups are generated by the termination of the cyclization reaction and dehydrogenation, which can cause structural defects in carbon fiber, such as chain scissions and point defects [20]. For Fe-PAN, unreacted and unsaturated nitrile groups remained, indicating insufficient cyclization of the PAN after thermal oxidative stabilization.

As mentioned above, oxidation generates free radicals in the PAN molecules during the stabilization process, which releases heat. As shown in Fig. 5 and Table 3, the DSC thermogram of raw-PAN in air exhibited a narrow and sharp peak at 296.3 °C. The onset temperature for raw-PAN was 292.8 °C (T_{on}), and the stabilization process progressed up to 298.9 °C (T_{off}). Here, the free radicals generated a large amount of heat ($\Delta H = -500$ J g^{-1}) in a temperature change (ΔT) of 6.1 °C. For the PAN molecules that bonded with transition metal ions, the exothermic peaks occurred at a lower temperature and the thermal oxidative process released more heat. However, the addition of Fe^{2+} and Ni^{2+} to PAN did not alleviate the intense heat generation. In the case of Fe-PAN, T_{on} was 265.4 °C and the stabilization process continued to 271.8 °C, with − 603 J g^{-1} of heat being released during the 6.4 °C (ΔT) increase. The addition of Fe^{2+} ions to PAN also aggravated the heat release rate during the thermal oxidative stabilization process, as shown in Table 3. In contrast, the addition of Co^{2+} or Cu^{2+} to PAN

Table 3 Differential scanning calorimetry (DSC) data of the heat released during the stabilization of raw PAN and PAN bonded with transition metal ions from 195 to 325 °C upon heating at 10 °C min^{-1} in air atmosphere

Sample	DSC in air					
	T_{on} (°C)	T_{off} (°C)	ΔT (°C)	T_p (°C)	ΔH (J g^{-1})	ΔH/ΔT (J g^{-1} °C^{-1})
Raw-PAN	292.8	298.9	6.1	296.3	− 500	81.97
Fe-PAN	265.4	271.8	6.4	269.6	− 603	94.21
Co-PAN	249.5	269.2	19.7	262	− 706	35.84
Ni-PAN	272.6	279.2	6.6	276.8	− 620	93.94
Cu-PAN	268.3	276.4	8.1	273.1	− 598	73.83

T_{on}: temperature at the onset of stabilization; T_{off}: temperature at the end of stabilization; ΔT: temperature change; T_p: peak temperature of stabilization; ΔH: enthalpy change

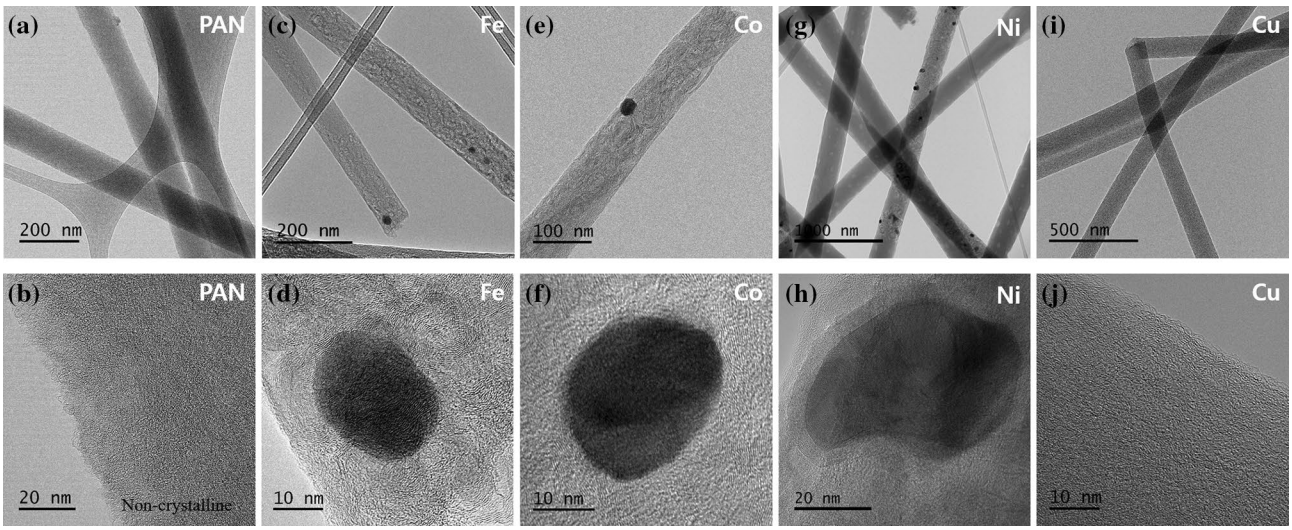

Fig. 6 TEM images of CNF **a**, **b** without any additive, with **c**, **d** iron, **e**, **f** cobalt, **g**, **h** nickel nanoparticles, and with **i**, **j** copper acetate monohydrate as addictive

resulted in a longer duration of heat release and a lower T_{on} for initiation of the thermal oxidative process (Fig. 5). The DSC peak of Cu-PAN was not only less intense but was also broader than those of Fe-PAN and Ni-PAN. This indicated that the exothermic reaction started from a lower temperature and the reaction proceeded without an intensive exothermic reaction as the temperature increased. The stabilization temperature of Cu-PAN ranged from 268.3 to 276.4 °C with a heat of − 598 J g^{-1} released. However, the DSC peak of Co-PAN appeared to be broader, spanning a wide temperature range rather than a narrow one. As shown in Table 3, the stabilization of Co-PAN was carried out from 249.5 to 269.2 °C (ΔT = 19.7 °C), with − 706 J g^{-1} of heat released. We examined the heat release rates of various thermal oxidative stabilization processes by dividing the amount of heat generated (during heating of the various PAN samples) by the reaction temperature range (ΔH/ΔT). It was determined that the addition of Co^{2+} and Cu^{2+} to PAN had resulted in the lowest rates of heat release from the exothermic reaction (Table 3).

After the thermal oxidative stabilization process, the stabilized PAN was annealed at 1000 °C with 100 sccm of Ar and 20 sccm of H_2 flowing. TEM images were taken to observe the effect of added transition metals on the microstructure of the carbon nanofiber, as shown in Fig. 6. No crystalline structure was found in the carbon fibers without any additives, as shown in Fig. 6a, b, which showed an almost amorphous carbon phase. On the contrary, carbon fibers containing Fe, Co and Ni have a partially graphitized structure (Fig. 6c–h). More specifically, the CNF contain different metals formed by different carbon crystal structures. As an example, the carbon structure of iron in Fig. 6c, d and Fig. S2 in the Supplementary Information resembled CNT [47, 48]. During the carbonization process, iron nanoparticles in CNF were spread and merged, while CNT structures were synthesized due to the catalytic effect of iron nanoparticles. Path traces of

the iron nanoparticle changed the amorphous carbon into a graphitic carbon structure similar to CNT (Fig. S2(a)) [49, 50]. In the case of cobalt shown in Fig. 6e, f and Fig. S3, the existing cobalt nanoparticles caused the formation of graphitic carbon with a crystalline structure similar to the graphite pockets in CNF [51]. In Fig. 6g, h, with nickel nanoparticles, the graphitic structure was only found on the nickel surface although the structure was well ordered. Finally, as shown in Fig. 6i, j, no copper nanoparticles were observed in the copper-containing CNFs, revealing the evaporation of copper during the high-temperature and low-pressure heat treatment. It showed only an amorphous carbon phase, just like CNF, without additives.

Raman spectroscopy was applied to compare the crystallinity depending on the additive transition metals. As shown in Fig. S4, Raman bands from 800 to 2000 cm^{-1} were fitted with the Lorentzian (G (1580 cm^{-1}), D1 (1350 cm^{-1}), D2 (1620 cm^{-1}), and D4 (1200 cm^{-1})) and Gaussian (D3 (1510 cm^{-1})) line shapes using Origin inbuilt fitting procedures. Consistent with the TEM data, CNF with iron and cobalt nanoparticles showed higher intensity of G-band and lower intensity of D3-band than the other CNFs, indicating the higher content of graphitic sp2 phase existed in CNF with iron and cobalt nanoparticles owing to their CNT-like and graphene-pocket-like graphitic structure observed from TEM, respectively (Fig. 6 and Figs. S2, S3). On the contrary, the D3-band presenting around 1510 cm^{-1} in less crystallized carbon materials such as amorphous carbon [52, 53] showed higher intensity in raw CNFs and in CNFs containing nickel and copper additives. This finding is also consistent with the crystalline structures observed by TEM measurement.

4 Conclusion

The structural evolution of electrospun PAN nanofibers bonded with different transition metal precursors was investigated through FTIR and DSC analyses. The cyclization rate and exothermic reaction of the thermal oxidative stabilization process were controlled differently depending on the various transition metal ions used. The addition of the transition metals to PAN generally decreased the stabilization temperature. With the exception of Fe-PAN, the transition metals increased the number of cyclization reactions. Notably, the additions of Co^{2+} and Cu^{2+} alleviated the extensive heat, initiating the thermal oxidative stabilization of PAN at a lower temperature. Specifically, although the exothermic reaction (ΔH) in Co-PAN stabilization was increased by approximately 140%, the heat release rate (ΔH/ΔT) was alleviated by approximately 44%. The addition of Fe^{2+} and Co^{2+} also improved the crystallinity of CNF in 1000 °C heat treatment in a low-pressure Ar and H_2 environment.

Supplementary Information The online version contains supplementary material available at https://doi.org/10.1007/s10904-021-01954-x.

Acknowledgements This work was supported by a grant from the Korea Evaluation Institute of Industrial Technology (KEIT) funded by the Ministry of Trade, Industry & Energy (MOTIE) [No. 20012341].

Code availability Not applicable.

Declarations

Conflict of interest The authors have no conflicts of interest to declare that are relevant to the content of this article.

References

1. H. Morgan, *Carbon Fibers and Their Composites* (CRC Press, Boca Raton, 2005).
2. J.B. Donnet, T.K. Wang, J.C. Peng, S. Rebouillat, *Carbon Fibers*, 3rd edn. (Marcel Dekker, New York, 1998).
3. E. Fitzer, *Carbon Fibers and Their Composites* (Spinger, New York, 1985).
4. D.D. Edie, Carbon **36**, 345–362 (1998)
5. E. Fitzer, Carbon **27**, 621–645 (1989)
6. E. Frank, F. Hermanutz, M.R. Buchmeiser, Macromol. Mater. Eng. **297**, 493–501 (2012)
7. O.-K. Park, S. Lee, H.-I. Joh, J.K. Kim, P.-H. Kang, J.H. Lee, B.-C. Ku, Polymer **53**, 2168–2174 (2012)
8. S. Chand, J. Mater. Sci. **35**, 1303–1313 (2000)
9. R.V. Ghorpade, D.W. Cho, S.C. Hong, Carbon **121**, 502–511 (2017)
10. N.U. Nguyen-Thai, S.C. Hong, Macromolecules **46**, 5882–5889 (2013)
11. Z. Fu, Y. Gui, S. Liu, Z. Wang, B. Liu, C. Cao, H. Zhang, J. Appl. Polym. Sci. **131**, 40834 (2014)
12. Y. Xue, J. Liu, J. Liang, Polym. Degrad. Stab. **98**, 219–229 (2013)
13. S.-P. Rwei, T.-F. Way, Y.-S. Hsu, Polym. Degrad. Stab. **98**, 2072–2080 (2013)
14. E.V. Loginova, I.V. Mikheev, D.S. Volkov, M.A. Proskurnin, Anal. Methods **8**, 371–380 (2016)
15. J. Hao, Y. Liu, C. Lu, Polym. Degrad. Stab. **147**, 89–96 (2018)
16. D.U. Park, N.K. Han, J.H. Ryu, W.H. Park, Y.G. Jeong, Fibers Polym. **19**, 2007–2015 (2018)
17. J.D. Moskowitz, W. Jacobs, A. Tucker, M. Astrove, B. Harmon, Polym. Degrad. Stab. **178**, 109198 (2020)
18. H. Liu, S. Zhang, J. Yang, M. Ji, J. Yu, M. Wang, X. Chai, B. Yang, C. Zhu, J. Xu, Polymers **11**, 1150 (2019)
19. G. Ayrey, S.K. Chadda, R.C. Poller, J. Polym. Sci. Polym. Chem. Ed. **20**, 2249–2258 (1982)
20. X. Qin, Y. Lu, H. Xiao, Y. Song, Mater. Lett. **76**, 162–164 (2012)
21. X. Li, A. Qin, X. Zhao, D. Liu, H. Wang, C. He, Phys. Chem. Chem. Phys. **17**, 21856–21865 (2015)
22. H.G. Chae, M.L. Minus, A. Rasheed, S. Kumar, Polymer **48**, 3781–3789 (2007)
23. M. Mohammadi, A. Rezaei, A. Khazaei, S. Xuwei, Z. Huajun, ACS Appl. Mater. Interfaces **11**, 33194–33206 (2019)
24. P. Hayati, S. Suárez-García, A. Gutierrez, E. Şahin, D.R. Molina, A. Morsali, A.R. Rezvani, Ultrason. Sonochem. **42**, 310–319 (2018)

25. A. Ansari, S. Vahedi, O. Tavakoli, M. Khoobi, M.A. Faramarzi, Appl. Organomet. Chem. **33**, e4634 (2019)
26. T. Mortezazadeh, E. Gholibegloo, N. Riyahi Alam, S. Haghgoo, A. Musa, M. Khoobi, J. Biomed. Phys. Eng. **10**, 25–38 (2020)
27. S. Okazoe, Y. Yasaka, M. Kudo, H. Maeno, Y. Murakami, Y. Kimura, Chem. Commun. **54**, 7834–7837 (2018)
28. Q. Bai, F.C. Shen, S.L. Li, J. Liu, L.Z. Dong, Z.M. Wang, Y.Q. Lan, Small Methods **2**, 1800049 (2018)
29. L. Xu, L. Zhang, B. Cheng, J. Yu, Carbon **152**, 652–660 (2019)
30. B. Zhang, Z.-L. Xu, Y.-B. He, S. Abouali, M.A. Garakani, E.K. Heidari, F. Kang, J.-K. Kim, Nano Energy **4**, 88–96 (2014)
31. B. Bajaj, H.-I. Joh, S.M. Jo, J.H. Park, K.B. Yi, S. Lee, Appl. Surf. Sci. **429**, 253–257 (2018)
32. H. Tang, W. Chen, J. Wang, T. Dugger, L. Cruz, D. Kisailus, Small **14**, 1703459 (2018)
33. M.A.A.M. Abdah, N.H.N. Azman, S. Kulandaivalu, Y. Sulaiman, Mater. Des. **186**, 108199 (2020)
34. Y. Chen, C. Zou, M. Mastalerz, S. Hu, C. Gasaway, X. Tao, Int. J. Mol. Sci. **16**, 30223–30250 (2015)
35. D. Koutsianitis, C. Mitani, K. Giagli, D. Tsalagkas, K. Halasz, O. Kolonics, C. Gallis, L. Csoka, Ultrason. Sonochem. **23**, 148–155 (2015)
36. H.-K. Lin, C.-B. Wang, H.-C. Chiu, S.-H. Chien, Catal. Lett. **86**, 63–68 (2003)
37. B. Minčeva-Šukarova, B. Mangovska, G. Bogoeva-Gaceva, V.M. Petruševski, Croat. Chem. Acta. **85**, 63–70 (2012)
38. J. Zhao, J. Zhang, T. Zhou, X. Liu, Q. Yuan, A. Zhang, RSC Adv. **6**, 4397–4409 (2016)
39. A. Barth, Prog. Biophys. Mol. Biol. **74**, 141–173 (2000)
40. X. Colom, F. Carrillo, F. Nogués, P. Garriga, Polym. Degrad. Stab. **80**, 543–549 (2003)
41. I.A. Mudunkotuwa, V.H. Grassian, Langmuir **30**, 8751–8760 (2014)
42. M. Wolpert, P. Hellwig, Spectrochim. Acta A Mol. Biomol. Spectrosc. **64**, 987–1001 (2006)
43. H. Kakida, K. Tashiro, Polym. J. **29**, 353–357 (1997)
44. Y. Liu, *Stabilization and Carbonization Studies of Polyacrylonitrile/Carbon Nanotube Composite Fibers* (Ph.D. Dissertation, School of Polymer, Textile, and Fiber Engineering, Georgia Institute of Technology, 2010)
45. M.A. Phadke, D.A. Musale, S.S. Kulkarni, S.K. Karode, J. Polym. Sci. Part B Polym. Phys. **43**, 2061–2073 (2005)
46. Y. Zhu, M.A. Wilding, S.K. Mukhopadhyay, J. Mater. Sci. **31**, 3831–3837 (1996)
47. B.A. Newcomb, L.A. Giannuzzi, K.M. Lyons, P.V. Gulgunje, K. Gupta, Y. Liu, M. Kamath, K. McDonald, J. Moon, B. Feng, Carbon **93**, 502–514 (2015)
48. K. Zhao, Z.-Y. Liu, B.-L. Xiao, D.-R. Ni, Z.-Y. Ma, Acta Metall. Sin. (Engl. Lett.) **31**, 134–142 (2018)
49. B.J. Mapleback, T.J. Simons, Y. Shekibi, K. Ghorbani, A.N. Rider, Electrochim. Acta **331**, 135233 (2020)
50. H. Wang, X. Li, F. Meng, G. Wang, D. Zhang, Chem. Eng. J. **392**, 123798 (2020)
51. T. Lehnert, M.K. Kinyanjui, A. Ladenburger, D. Rommel, K. Wörle, F. Börrnert, K. Leopold, U. Kaiser, ACS Nano **11**, 7967–7973 (2017)
52. D.G. Henry, I. Jarvis, G. Gillmore, M. Stephenson, Earth Sci. Rev. **198**, 102936 (2019)
53. M. Pawlyta, J.-N. Rouzaud, S. Duber, Carbon **84**, 479–490 (2015)

Authors and Affiliations

Jung-Hun Lee[1] · Siying Li[1] · Ji-Beom Yoo[1,2] · Young-Jun Kim[1,3]

✉ Ji-Beom Yoo
jbyoo@skku.edu

✉ Young-Jun Kim
yjkim68@skku.edu

[1] SKKU Advanced Institute of Nanotechnology (SAINT), Sungkyunkwan University, Suwon 16419, Republic of Korea

[2] School of Advanced Materials Science and Engineering, Sungkyunkwan University, Suwon 16419, Republic of Korea

[3] Department of Nano Engineering, Sungkyunkwan University, Suwon 16419, Republic of Korea